Letter | Editors' Suggestion

# Height-conserving quantum dimer models

Zheng Yan,[1] Zi Yang Meng,[1,*] David A. Huse,[2,3] and Amos Chan[4,†]

[1]*Department of Physics and HKU-UCAS Joint Institute of Theoretical and Computational Physics, The University of Hong Kong, Pokfulam Road, Hong Kong, China*

[2]*Department of Physics, Princeton University, Princeton, New Jersey 08544, USA*

[3]*Institute for Advanced Study, Princeton, New Jersey 08540, USA*

[4]*Princeton Center for Theoretical Science, Princeton University, Princeton, New Jersey 08544, USA*

(Received 29 April 2022; revised 10 July 2022; accepted 12 July 2022; published 26 July 2022)

We propose a height-conserving quantum dimer model (hQDM) such that the lattice sum of its associated height field is conserved, and that it admits a Rokhsar-Kivelson (RK) point. The hQDM with a minimal interaction range on the square lattice exhibits Hilbert space fragmentation and maps exactly to the XXZ spin model on the square lattice in certain Krylov subspaces. We obtain the ground-state phase diagram of hQDM via quantum Monte Carlo simulations, and demonstrate that a large portion of it is within the Krylov subspaces which admit the exact mapping to the XXZ model, with dimer ordered phases corresponding to easy-axis and easy-plane spin orders. At the RK point, the apparent dynamical exponents obtained from the single mode approximation and the height correlation function show drastically different behavior across the Krylov subspaces, exemplifying Hilbert space fragmentation and emergent glassy phenomena.

DOI: 10.1103/PhysRevB.106.L041115

*Introduction.* Quantum dimer models (QDMs) [1] are paradigmatic models of strongly correlated systems subject to strong local constraints. Originally introduced to model the physics of short-range resonating valence bond states [2–4], QDMs have subsequently been shown to host a plethora of phenomena, such as topological order and fractionalization [5–8], mapping to height models [9–11], unconventional phase transition with anyon condensation [12–16], emergent continuous symmetry and gauge field [15,16], and more [17–27]. On the other hand, recent experimental progress in ultracold atomic gases [16,28–31] has led to a surge of interest in understanding nonequilibrium dynamics in closed quantum many-body systems, including quantum many-body chaos [32–38], many-body localization [39–42], quantum many-body scars [43–49], anomalous dynamics and subdiffusive behavior [50–57], localization in fractonic systems [58–62], and Hilbert space fragmentation (HSF) [63–76], the latter of which provide examples of nonintegrable systems which fail to obey the eigenstate thermalization hypothesis [77–79].

In this Letter, guided by the connection between constrained dynamics and height-conserving field theories uncovered in Ref. [53], we design a height-conserving quantum dimer model (hQDM) that displays phenomena of constrained systems, in particular HSF, yet retains the attractive features of QDM described above. Specifically, for the square-lattice hQDM with minimal-range interactions, we show that the conservation of its associated height field leads to HSF, and that there exists an exact mapping between hQDM and a XXZ spin model in certain Krylov subspaces (KSs). We employ the unbiased sweeping cluster quantum Monte Carlo (QMC) simulation [15,16,80,81] to obtain the ground-state phase diagram and find the main part of the phase diagram can be characterized by that of the two-dimensional XXZ model, with different dimer ordering corresponding to easy-axis and easy-plane spin long-range orders. At the RK point, the apparent dynamical exponents obtained from the single mode approximation and the height correlation of QMC data, exhibit drastically different behavior across the KS. These results confirm the fragmented Hilbert space and emergent glassy behavior of our model and its relevance to further developments of constrained quantum lattice models is discussed.

*Model.* Consider close-packed tiling of dimers on a square (bipartite) lattice, such that each site is occupied by exactly one dimer. For each dimer configuration, one can construct a mapping to a height field $h(\mathbf{x})$, which we review in the Supplemental Material (SM) [82]. We introduce a height-conserving QDM such that (i) it admits a general Rokhsar-Kivelson (RK) point [1] in its parameter space, and (ii) the sum of its associated height field $h(\mathbf{x})$ is conserved. We focus on the Hamiltonian $H = H_{\text{res}} + H_{\text{diag}}$ with an interaction of *minimal* range on the square lattice, where

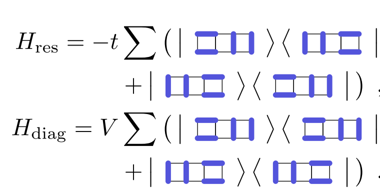
(1)

*zymeng@hku.hk
†amos.chan@princeton.edu

 

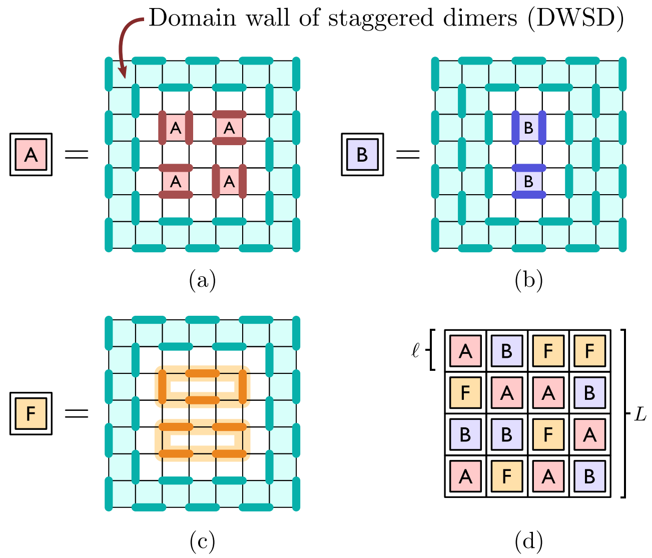


FIG. 1. (a), (b) DWSD (in cyan) surrounding regions of flippable plaquettes residing in sublattices A and B, respectively. (c) DWSD surrounding a region of inactive dimer configuration. Loop updates on the orange loops will generate additional inactive configurations exponential in the region size. (d) $O(\gamma^{L^2})$ number of KSs with isolated active regions can be constructed by piecing (a)–(c) together with $\gamma > 1$.

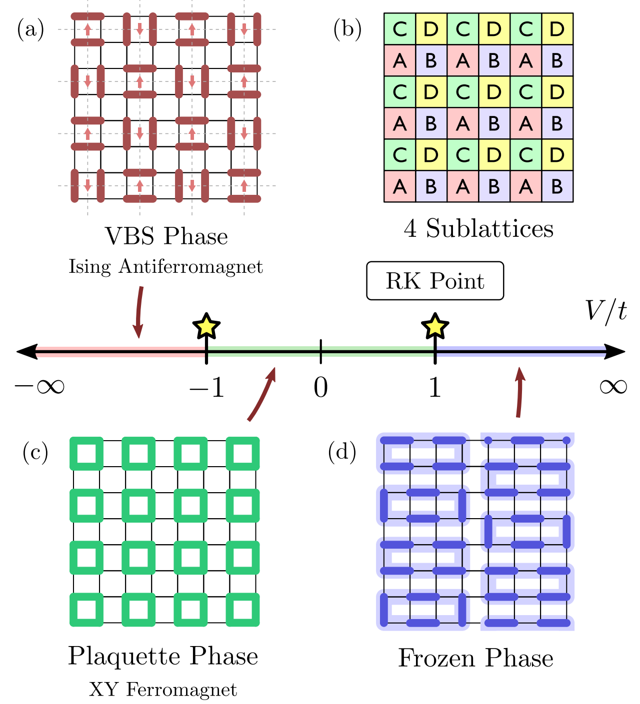


FIG. 2. Phase diagram of the minimal-range hQDM on the square lattice. For $V/t \in (-\infty, -1)$, the system is in a VBS phase, with eight degenerate ground states generated by performing plaquette flips and translations of the pattern (a) to four sublattices defined in (b). The hQDM restricted to the KS of (a) can be exactly mapped to the XXZ model, where the VBS is the Ising antiferromagnetic phase. For $V/t \in (-1, 1)$, the system is in the plaquette phase illustrated in (c), corresponding to the XY ferromagnetic phase of the XXZ model. For $V/t \in (1, \infty)$, the system is in the frozen phase and has $O(e^{L^2})$ number of inactive and degenerate GSs, some of which can be generated by performing loop updates on (d). The transition point between VBS and plaquette phases is equivalent to the antiferromagnetic Heisenberg point of the XXZ model and that between the plaquette and frozen phases is the RK point.

The sums are over all possible vertically or horizontally aligned next-to-nearest-neighbor plaquette pairs. hQDM with interactions of longer range and/or conserved height multipoles [82] are amenable to field-theoretical analysis, which we discuss in detail in a forthcoming work [83]. As the QDM, the hQDM preserves the *tilts* or *winding numbers*, defined in terms of the height field as $t_1 = [h(\mathbf{x} = (L, x_2)) - h(\mathbf{x} = (0, x_2))]/L$ and $t_2 = [h(\mathbf{x} = (x_1, L)) - h(\mathbf{x} = (x_1, 0))]/L$ for any values of $x_1$ and $x_2$. Additionally, the short-range nature of the pairwise plaquette flips of $H^{(0)}_{\text{res}}$ leads to extra conserved quantities, namely the total height $I_X$ for each sublattice, $\{X = \text{A, B, C, D}\}$, shown in Fig. 2(b). Together, the set of conserved charges is $\{t_1, t_2, I_\text{A}, I_\text{B}, I_\text{C}, I_\text{D}\}$.

*Hilbert space fragmentation.* Our hQDM has HSF, i.e., the full space of states breaks into dynamically disconnected KSs. A *Krylov subspace* (KS) is defined as $\mathcal{K}(H, |\psi\rangle) = \text{span}\{H^n|\psi\rangle, n \in \mathbb{N}\} \equiv \mathcal{K}(|\psi\rangle)$ with size $D_\mathcal{K}$, and in our context, the basis states $|\psi\rangle$ are dimer configurations. A system is said to exhibit HSF [63–65] if $\mathcal{K}(H, |\psi\rangle)$ does not span the Hilbert subspace labeled by the symmetry quantum numbers of $|\psi\rangle$. In our minimal-range hQDM, we prove in SM [82] that there exists an exponential number (in system size) of subsectors with (i) $D_\mathcal{K} = 1$ (frozen KS), (ii) $D_\mathcal{K} = O(1)$ (minimally active KS), and (iii) $D_\mathcal{K} = O(\alpha^{L^2})$ (active KS) with constant $\alpha > 1$. The idea of the proof is demonstrated in a construction using a *domain wall of staggered dimers* (DWSD) (see Fig. 1), defined as a connected region of plaquettes where no plaquettes are occupied by a parallel dimer pair. A DWSD is a "blockade" since regions separated by DWSD are dynamically disconnected in that no terms in $H$ can act nontrivially on or across the DWSD. Claims (i)–(iii) are then proven by obtaining distinct KS via piecing multiple blocks of active or inactive dimer configurations surrounded by DWSD, shown in Fig. 1 and SM [82]. We also have strong indications, but not a proof, as discussed below, that this minimal-range hQDM has strong HSF, so no KS has an entropy density equal to the full entropy density.

*Phase diagram.* We can obtain the phase diagram (Fig. 2) of our minimal-range hQDM in several tractable limits. For $V/t \to -\infty$, the Hamiltonian favors states with the most number of flippable plaquette pairs. Such a state is shown in Fig. 2(a), and we prove in SM [82] that there are eight degenerate ground states (GSs) generated by (i) performing pair-dimer rotation on all plaquettes with parallel dimers, and (ii) translating the pattern [Fig. 2(a)] to the four sublattices [Fig. 2(b)]. Furthermore, these eight degenerate GSs belong to four (disconnected) KSs associated with each sublattice [82]. We refer to these GSs as the valence bond solid (VBS).

For $V/t \in (1, \infty)$, the Hamiltonian favors states without any flippable plaquette pairs, i.e., the system is in the frozen phase. We explicitly construct degenerate GS with extensive entropy in Fig. 2(d), generated by performing loop updates—by flipping occupied links to unoccupied links in a given loop, and vice versa—on each blue loop [82]. Each of such states forms a KS of size one. Note that all inactive configurations in QDM are also valid inactive configurations in hQDM. However, unlike QDM, hQDM has extensive GS entropy in the frozen phase while QDM has subextensive GS entropy in the staggered phase for $V/t \in (1, \infty)$, and the degenerate hQDM GSs contain states with a variety of height tilts, including the columnar states with zero tilt.

At $V/t = 1$, as in QDM, hQDM has a RK point [1,10,11]. The GSs at the RK point are highly degenerate, with a unique GS from each KS given by $|\mathrm{GS}\rangle_{\mathcal{K}} \propto \sum_{C\in\mathcal{K}} |C\rangle$. The field-theoretical approaches at the RK point will be discussed in detail in Ref. [83]. Away from the RK point, one can consider the following heuristic argument to justify the frozen and VBS phases: With $V/t \to 1^{+}$, subspaces without any flippable plaquettes have the lowest energy, consistent with the frozen phase; with $V/t \to 1^{-}$, the lowest-energy subspaces should be the ones with the most flippable plaquettes, i.e., the KS where VBSs reside.

There exists an exact mapping between our minimal-range hQDM and XXZ spin models in a certain set of KSs, $\mathcal{K}(|\psi\rangle_X)$, where all flippable plaquettes in $|\psi\rangle_X$ are residing on the same sublattice $X \in \{\mathrm{A, B, C, D}\}$ via $|\text{▯}\rangle_{\mathbf{x}} \xrightarrow{g} |\downarrow\rangle_{\tilde{\mathbf{x}}}$, $|\text{▭}\rangle_{\mathbf{x}} \xrightarrow{g} |\uparrow\rangle_{\tilde{\mathbf{x}}}$, where $\mathbf{x}$ and $\tilde{\mathbf{x}}$ labels the plaquettes of the original lattice and of sublattice $X$, respectively [82]. The validity of this mapping relies on the fact that flippable plaquettes in these KSs always remain in the same sublattice under the action of $H$. Therefore, it maps a $2L \times 2L$ hQDM into a $L \times L$ XXZ model in certain subspaces,

$$H_{\mathrm{hQDM}}|_{\mathcal{K}(|\psi\rangle_X),\{\mathbf{x}\}} = H_{\mathrm{XXZ}}|_{\mathcal{K}[g(|\psi\rangle_X)],\{\tilde{\mathbf{x}}\}}, \tag{2}$$

and

$$H_{\mathrm{XXZ}}|_{\{\tilde{\mathbf{x}}\}} = -t \sum_{\langle \tilde{\mathbf{x}}, \tilde{\mathbf{x}}'\rangle} \left(S^{+}_{\tilde{\mathbf{x}}} S^{-}_{\tilde{\mathbf{x}}'} + S^{-}_{\tilde{\mathbf{x}}} S^{+}_{\tilde{\mathbf{x}}'}\right) + \frac{V}{2} \sum_{\langle \tilde{\mathbf{x}}, \tilde{\mathbf{x}}'\rangle} \left(1 - S^{z}_{\tilde{\mathbf{x}}} S^{z}_{\tilde{\mathbf{x}}'}\right), \tag{3}$$

where $S^{\alpha}_{\tilde{\mathbf{x}}}$ with $\alpha = x, y, z$ are the Pauli matrices, and $S^{\pm} = \frac{1}{2}(S^{x} \pm iS^{y})$. Note that when longer-range terms of hQDM are introduced, this mapping is no longer valid as the relevant KSs have enlarged. However, for the minimal-range hQDM, this XXZ description is crucial in describing the phase diagram for $V/t \in (-\infty, 1)$.

*Sweeping cluster quantum Monte Carlo on hQDM.* We employ the sweeping cluster QMC algorithm [80,81] to simulate the phase diagram. The method has recently been intensively applied on the square and triangle lattice QDM models to map out the GS phase diagram and extract the low-energy excitations [15,16,84]. The method not only respects the local constraint in hQDM between each QMC update, but also allows for loop updates with randomly sampled loops, ensuring different subspaces labeled by $\{t_1, t_2, I_{\mathrm{A}}, I_{\mathrm{B}}, I_{\mathrm{C}}, I_{\mathrm{D}}\}$ and the fragmented KSs within being sampled. We simulated the hQDM with linear system sizes up to $L = 24$, and the inverse temperature $\beta = L$.

Our QMC data show that the GSs in $V/t \in (-\infty, 1)$ indeed reside in KSs described by the mapping in Eq. (2). To probe the phase diagram, we study the dimer-pair structure factor

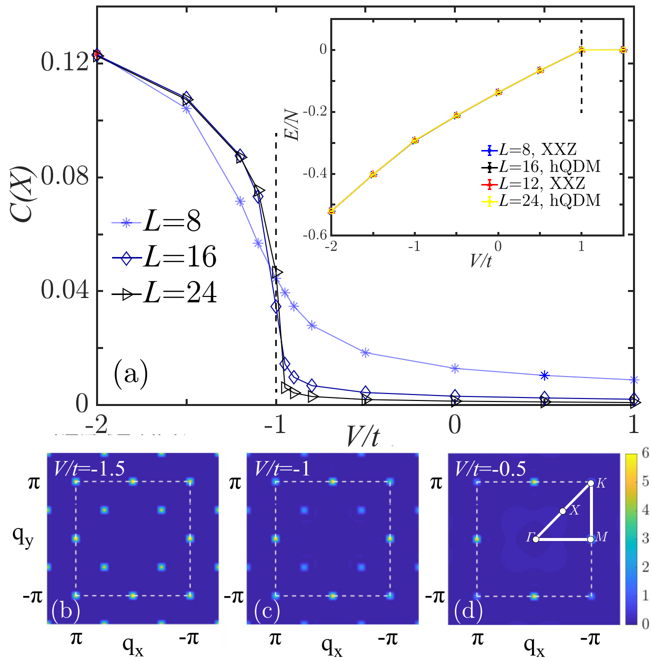


FIG. 3. (a) The dimer-pair structure factor $C(X)$ for hQDM shows a first-order transition from VBS (Ising antiferromagnet in the XXZ model) to the plaquette (XY ferromagnet in the XXZ model) phase at $V = -1$. The inset shows the energy density of hQDM with $L = 16, 24$ and of the XXZ model with $L = 8, 12$ as a function of $V/t$. The curves coincide and exhibit a transition at the RK point $V = 1$. (b)–(d) are the dimer-pair structure factors at $V = -1.5, -1$, and $-0.5$ inside the Brillouin zone, respectively. With $C(\mathbf{q})$ peaks at $X$ and $M$ in (b) and (c), but only peak at $M$ in (d). The high-symmetry path is denoted in (d).

$C_{ij}(\mathbf{q})$, defined as the Fourier transform of the pair dimer correlation function $C_{ij,\mathbf{x}-\mathbf{x}'} = \frac{\langle \mathcal{D}_{i\mathbf{x}} \mathcal{D}_{j,\mathbf{x}'}\rangle - \langle \mathcal{D}_{i,\mathbf{x}}\rangle\langle \mathcal{D}_{j,\mathbf{x}'}\rangle}{\langle \mathcal{D}^2_{i,\mathbf{x}'}\rangle - \langle \mathcal{D}_{i,\mathbf{x}'}\rangle^2}$, where $\mathcal{D}_{i,\mathbf{x}}$ with $i = \text{▭}, \text{▯}$ is the projector of vertically or horizontally aligned dimer pairs at plaquette $\mathbf{x}$ [82]. The $C(\mathbf{q} = X)$ where $X = (\pi/2, \pi/2)$ and $i = j = \text{▭}$ serves as the square of the order parameter for the VBS phase. As shown in Fig. 3(a), as $V/t$ increases from $-\infty$, the hQDM undergoes a first-order phase transition [85] at $V/t = -1$ from the VBS phase [$C(X)$ is finite] to a plaquette phase [$C(X)$ is zero] in one of the four sublattices. The same information is revealed in the $C(\mathbf{q})$ in the Brillouin zone (BZ) in Figs. 3(b)–3(d), where the structure peak at $X$ appears at $V = -1.5$ (we note here the peaks at $M$ and $K$ are due to the repetition of that at $X$) and $V = -1$ (here the peaks at $M$ and $X$ are due to the coexistence of VBS and plaquette phases), but at $V = -0.5$, when the system is inside the plaquette phase, $C(\mathbf{q})$ only develops peaks at $M = (\pi, 0)$ points.

This transition in hQDM corresponds to the transition from antiferromagnetic Ising phase to XY phase in the XXZ model in each of the KSs corresponding to the four sublattices. At the Heisenberg point $V = -1$, the $O(3)$ symmetry is recovered and the GS spontaneously break this symmetry, resulting in the coexistence of peak at $X$ and $M$ in Fig. 3(c). Similar phenomena have been seen in the context of deconfined quantum critical points and dimerized quantum magnets [86,87].

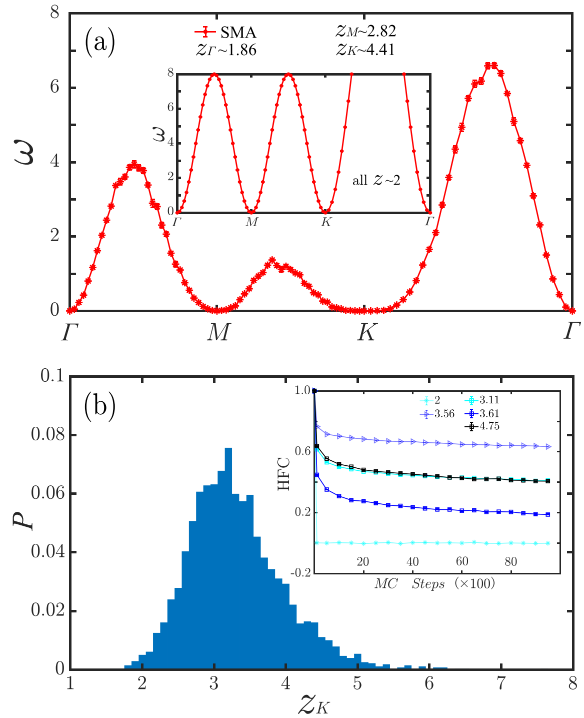


FIG. 4. (a). The dispersion of hQDM at the RK point in a random sector is given along the high-symmetry path, with the $z_{\mathbf{q}}$ denoted. The inset shows the dispersion in the XXZ sector, with all $z = 2$. (b). The distribution of $z_K$ for hQDM via random walk MC and SMA, where the distribution is obtained via 3000 randomly chosen sectors. The inset shows the real-space height field autocorrelation function of the A sublattice in different KSs with different $z_K$ (as labeled in the figure) against MC steps.

Moreover, we also compare the GS energy density from sweeping cluster QMC on hQDM, with that from directed loop QMC simulation [88–90] on the XXZ model. As shown in the inset of Fig. 3(a), two energies are identical, meaning the hQDM GS indeed resides in the XXZ KS, where the mapping to the XXZ model is valid. Interestingly, at $V/t \geqslant 1$, when the system is at the RK point and in the frozen phase, our QMC data show the mapping remains valid. Indeed, the ferromagnetic phase of the XXZ model (when $V/t > 1$) can be mapped to the columnar phase of the square-lattice QDM at $V/t > 1$ [91], which is one of the degenerate GSs in the frozen phase of hQDM.

*Dispersion and dynamic properties.* We finally study low-lying excitations at the RK point of the minimal-range hQDM where each sector has a zero-energy ground state, and show that the apparent dynamical exponent $z$ varies strongly between KS and the system develops emergent glassy behavior, indicating strong HSF.

We utilize the single mode approximation (SMA) upon QMC data to approximate a dimer dispersion [92,93]. Besides the low-energy dispersion, via the random walk method, we also sample KSs randomly and obtain the distribution of apparent dynamical exponents $z_{\mathbf{q}}$ at various $\mathbf{q}$ points in the BZ.

Our results are shown in Fig. 4. Different from the QDM, the dynamics of hQDM are extremely sensitive to KSs. In the XXZ KS which hosts the ground state for $V < t$, the dynamic exponent $z = 2$ (similar to that of the QDM [92]), all the exponents near $K$ are indeed close to 2 as shown in the inset of Fig. 4(a) [94]. However, the hQDM dispersion in the other KS [the main panel of Fig. 4(a)] clearly acquire larger apparent $z$. We further plot the distribution of $z_{K=(\pi,\pi)}$ extracted from the dispersion from sampling different sectors in Fig. 4(b), which exhibits a wide distribution centered around $z = 3$. Such behavior suggests strong fragmentation, since randomly chosen states do not appear to be in the same KS with any significant probability. We expect that the model will only have weak HSF upon inclusion of longer-range terms in Eq. (1).

We also study the autocorrelation function of height field at RK points using classical MC, by updating dimer configurations via the $H_{\text{res}}$ on a randomly chosen position from a initial state of certain sector. The measurement of height autocorrelation along the Monte Carlo steps (MCS) in one sublattice is shown in the inset of Fig. 4(b). In the XXZ sector, $z_K \sim 2$, autocorrelation decays very fast with ergodicity in the related Hilbert subspace. In other sectors, $z_K > 2$, the autocorrelation decays much slower which hinders the relaxation. There seems to be no obvious relationship between the autocorrelation decay and $z_K$. It is strong evidence for the glassy behavior which emerges in most sectors of hQDM.

*Conclusion and outlook.* In this Letter, we introduced the hQDM as a realization of height-conserving models. Rich phenomena such as HSF with DWSD as blockades, mapping to the XXZ model, and the emergent glassy behavior at the RK are observed analytically and numerically. The hQDM height field theory [10,11], lattice gauge theory, Lifshitz models, and conformal critical point [95] will be presented in upcoming work [83]. Emergent fractonic behavior [96–101], explored recently in dimer models in higher than two dimensions [102,103], the nature of the low-lying excitations, and the structure of HSF in hQDM with interactions of various ranges are also interesting open directions.

*Acknowledgments.* We wish to thank Jie Wang and Shivaji Sondhi for useful discussions, and Sanjay Moudgalya and Abhinav Prem for previous collaboration. Z.Y. and Z.Y.M. acknowledge support from the RGC of Hong Kong SAR of China (Grants No. 17303019, No. 17301420, No. 17301721, and No. AoE/P-701/20), the K. C. Wong Education Foundation (Grant No. GJTD-2020-01), and the Seed Funding "Quantum-Inspired explainable-AI" at the HKU-TCL Joint Research Centre for Artificial Intelligence. We thank the Information Technology Services at the University of Hong Kong and the Tianhe platforms at the National Supercomputer Centers in Guangzhou for technical support and generous allocation of CPU time. The authors acknowledge Beijng PARATERA Tech Company, Ltd. [104] for providing HPC resources that have contributed to the research results reported within this Letter. D.A.H. is supported in part by NSF QLCI Grant No. OMA-2120757. A.C. is supported by fellowships from the Croucher Foundation and the PCTS at Princeton University.

[1] D. S. Rokhsar and S. A. Kivelson, Superconductivity and the Quantum Hard-Core Dimer Gas, Phys. Rev. Lett. **61**, 2376 (1988).
[2] P. W. Anderson, The resonating valence bond state in $La_2CuO_4$ and superconductivity, Science **235**, 1196 (1987).
[3] P. Fazekas and P. W. Anderson, On the ground state properties of the anisotropic triangular antiferromagnet, Philos. Mag. **30**, 423 (1974).
[4] S. A. Kivelson, D. S. Rokhsar, and J. P. Sethna, Topology of the resonating valence-bond state: Solitons and high-$T_c$ superconductivity, Phys. Rev. B **35**, 8865 (1987).
[5] R. Moessner and S. L. Sondhi, Resonating Valence Bond Phase in the Triangular Lattice Quantum Dimer Model, Phys. Rev. Lett. **86**, 1881 (2001).
[6] G. Misguich, D. Serban, and V. Pasquier, Quantum Dimer Model on the Kagome Lattice: Solvable Dimer-Liquid and Ising Gauge Theory, Phys. Rev. Lett. **89**, 137202 (2002).
[7] R. Moessner, S. L. Sondhi, and E. Fradkin, Short-ranged resonating valence bond physics, quantum dimer models, and Ising gauge theories, Phys. Rev. B **65**, 024504 (2001).
[8] Z. Yan, X. Ran, Y.-C. Wang, R. Samajdar, J. Rong, S. Sachdev, Y. Qi, and Z. Y. Meng, Fully packed quantum loop model on the triangular lattice: Hidden vison plaquette phase and cubic phase transitions, arXiv:2205.04472.
[9] B. Nienhuis, H. J. Hilhorst, and H. W. J. Blote, Triangular SOS models and cubic-crystal shapes, J. Phys. A: Math. Gen. **17**, 3559 (1984).
[10] C. L. Henley, Relaxation time for a dimer covering with height representation, J. Stat. Phys. **89**, 483 (1997).
[11] C. L. Henley, From classical to quantum dynamics at Rokhsar–Kivelson points, J. Phys.: Condens. Matter **16**, S891 (2004).
[12] A. Ralko, M. Ferrero, F. Becca, D. Ivanov, and F. Mila, Zero-temperature properties of the quantum dimer model on the triangular lattice, Phys. Rev. B **71**, 224109 (2005).
[13] A. Ralko, M. Ferrero, F. Becca, D. Ivanov, and F. Mila, Dynamics of the quantum dimer model on the triangular lattice: Soft modes and local resonating valence-bond correlations, Phys. Rev. B **74**, 134301 (2006).
[14] X. Plat, F. Alet, S. Capponi, and K. Totsuka, Magnetization plateaus of an easy-axis kagome antiferromagnet with extended interactions, Phys. Rev. B **92**, 174402 (2015).
[15] Z. Yan, Y.-C. Wang, N. Ma, Y. Qi, and Z. Y. Meng, Topological phase transition and single/multi anyon dynamics of $Z_2$ spin liquid, npj Quantum Mater. **6**, 39 (2021).
[16] Z. Yan, R. Samajdar, Y.-C. Wang, S. Sachdev, and Z. Y. Meng, Triangular lattice quantum dimer model with variable dimer density, arXiv:2202.11100.
[17] M. Punk, A. Allais, and S. Sachdev, Quantum dimer model for the pseudogap metal, Proc. Natl. Acad. USA Sci. **112**, 9552 (2015).
[18] T. Oakes, S. Powell, C. Castelnovo, A. Lamacraft, and J. P. Garrahan, Phases of quantum dimers from ensembles of classical stochastic trajectories, Phys. Rev. B **98**, 064302 (2018).
[19] Z. Lan, M. van Horssen, S. Powell, and J. P. Garrahan, Quantum Slow Relaxation and Metastability due to Dynamical Constraints, Phys. Rev. Lett. **121**, 040603 (2018).
[20] J. Feldmeier, F. Pollmann, and M. Knap, Emergent Glassy Dynamics in a Quantum Dimer Model, Phys. Rev. Lett. **123**, 040601 (2019).
[21] R. Kobayashi, K. Shiozaki, Y. Kikuchi, and S. Ryu, Lieb-Schultz-Mattis type theorem with higher-form symmetry and the quantum dimer models, Phys. Rev. B **99**, 014402 (2019).
[22] H. Théveniaut, Z. Lan, G. Meyer, and F. Alet, Transition to a many-body localized regime in a two-dimensional disordered quantum dimer model, Phys. Rev. Research **2**, 033154 (2020).
[23] J. Lloyd, S. Biswas, S. H. Simon, S. A. Parameswaran, and F. Flicker, Statistical mechanics of dimers on quasiperiodic tilings, arXiv:2103.01235.
[24] J. Wildeboer, A. Seidel, N. S. Srivatsa, A. E. B. Nielsen, and O. Erten, Topological quantum many-body scars in quantum dimer models on the kagome lattice, Phys. Rev. B **104**, L121103 (2021).
[25] F. Pietracaprina and F. Alet, Probing many-body localization in a disordered quantum dimer model on the honeycomb lattice, SciPost Phys. **10**, 044 (2021).
[26] S. Powell, Quantum Kasteleyn transition, Phys. Rev. B **105**, 064413 (2022).
[27] B. Dabholkar, G. J. Sreejith, and F. Alet, Re-entrance effect in the high-temperature critical phase of the quantum dimer model on the square lattice, arXiv:2207.03301.
[28] G. Semeghini, H. Levine, A. Keesling, S. Ebadi, T. T. Wang, D. Bluvstein, R. Verresen, H. Pichler, M. Kalinowski, R. Samajdar, A. Omran, S. Sachdev, A. Vishwanath, M. Greiner, V. Vuletić, and M. D. Lukin, Probing topological spin liquids on a programmable quantum simulator, Science **374**, 1242 (2021).
[29] K. J. Satzinger, Y.-J. Liu, A. Smith, C. Knapp, M. Newman, C. Jones, Z. Chen, C. Quintana, X. Mi, A. Dunsworth, C. Gidney, I. Aleiner, F. Arute, K. Arya, J. Atalaya, R. Babbush, J. C. Bardin, R. Barends, J. Basso, A. Bengtsson *et al.*, Realizing topologically ordered states on a quantum processor, Science **374**, 1237 (2021).
[30] R. Verresen, M. D. Lukin, and A. Vishwanath, Prediction of Toric Code Topological Order from Rydberg Blockade, Phys. Rev. X **11**, 031005 (2021).
[31] R. Samajdar, W. W. Ho, H. Pichler, M. D. Lukin, and S. Sachdev, Quantum phases of Rydberg atoms on a kagome lattice, Proc. Natl. Acad. Sci. USA **118**, e2015785118 (2021).
[32] A. Nahum, J. Ruhman, S. Vijay, and J. Haah, Quantum Entanglement Growth under Random Unitary Dynamics, Phys. Rev. X **7**, 031016 (2017).
[33] A. Nahum, S. Vijay, and J. Haah, Operator Spreading in Random Unitary Circuits, Phys. Rev. X **8**, 021014 (2018).
[34] C. W. von Keyserlingk, T. Rakovszky, F. Pollmann, and S. L. Sondhi, Operator Hydrodynamics, OTOCs, and Entanglement Growth in Systems without Conservation Laws, Phys. Rev. X **8**, 021013 (2018).
[35] A. Chan, A. De Luca, and J. T. Chalker, Solution of a Minimal Model for Many-Body Quantum Chaos, Phys. Rev. X **8**, 041019 (2018).
[36] A. Chan, A. De Luca, and J. T. Chalker, Spectral Statistics in Spatially Extended Chaotic Quantum Many-Body Systems, Phys. Rev. Lett. **121**, 060601 (2018).
[37] A. Chan, A. De Luca, and J. T. Chalker, Eigenstate Correlations, Thermalization, and the Butterfly Effect, Phys. Rev. Lett. **122**, 220601 (2019).
[38] A. Kitaev, A simple model of quantum holography, KITP Strings Seminar and Entanglement (2015), https://online.kitp.ucsb.edu/online/entangled15/kitaev/.

[39] I. V. Gornyi, A. D. Mirlin, and D. G. Polyakov, Interacting Electrons in Disordered Wires: Anderson Localization and Low-$T$ Transport, Phys. Rev. Lett. **95**, 206603 (2005).
[40] D. M. Basko, I. L. Aleiner, and B. L. Altshuler, Metal insulator transition in a weakly interacting many-electron system with localized single-particle states, Ann. Phys. **321**, 1126 (2006).
[41] A. Pal and D. A. Huse, Many-body localization phase transition, Phys. Rev. B **82**, 174411 (2010).
[42] R. Nandkishore and D. A. Huse, Many-body localization and thermalization in quantum statistical mechanics, Annu. Rev. Condens. Matter Phys. **6**, 15 (2015).
[43] N. Shiraishi and T. Mori, Systematic Construction of Counterexamples to the Eigenstate Thermalization Hypothesis, Phys. Rev. Lett. **119**, 030601 (2017).
[44] S. Moudgalya, S. Rachel, B. A. Bernevig, and N. Regnault, Exact excited states of nonintegrable models, Phys. Rev. B **98**, 235155 (2018).
[45] C. J. Turner, A. A. Michailidis, D. A. Abanin, M. Serbyn, and Z. Papić, Weak ergodicity breaking from quantum many-body scars, Nat. Phys. **14**, 745 (2018).
[46] S. Moudgalya, N. Regnault, and B. A. Bernevig, Entanglement of exact excited states of Affleck-Kennedy-Lieb-Tasaki models: Exact results, many-body scars, and violation of the strong eigenstate thermalization hypothesis, Phys. Rev. B **98**, 235156 (2018).
[47] C. J. Turner, A. A. Michailidis, D. A. Abanin, M. Serbyn, and Z. Papić, Quantum scarred eigenstates in a Rydberg atom chain: Entanglement, breakdown of thermalization, and stability to perturbations, Phys. Rev. B **98**, 155134 (2018).
[48] W. W. Ho, S. Choi, H. Pichler, and M. D. Lukin, Periodic Orbits, Entanglement, and Quantum Many-Body Scars in Constrained Models: Matrix Product State Approach, Phys. Rev. Lett. **122**, 040603 (2019).
[49] V. Khemani, C. R. Laumann, and A. Chandran, Signatures of integrability in the dynamics of Rydberg-blockaded chains, Phys. Rev. B **99**, 161101(R) (2019).
[50] J. Feldmeier, P. Sala, G. De Tomasi, F. Pollmann, and M. Knap, Anomalous Diffusion in Dipole- and Higher-Moment-Conserving Systems, Phys. Rev. Lett. **125**, 245303 (2020).
[51] S. Scherg, T. Kohlert, P. Sala, F. Pollmann, B. Hebbe Madhusudhana, I. Bloch, and M. Aidelsburger, Observing non-ergodicity due to kinetic constraints in tilted Fermi-Hubbard chains, Nat. Commun. **12**, 4490 (2021).
[52] A. Morningstar, V. Khemani, and D. A. Huse, Kinetically constrained freezing transition in a dipole-conserving system, Phys. Rev. B **101**, 214205 (2020).
[53] S. Moudgalya, A. Prem, D. A. Huse, and A. Chan, Spectral statistics in constrained many-body quantum chaotic systems, Phys. Rev. Research **3**, 023176 (2021).
[54] J. Iaconis, A. Lucas, and R. Nandkishore, Multipole conservation laws and subdiffusion in any dimension, Phys. Rev. E **103**, 022142 (2021).
[55] J. Feldmeier and M. Knap, Critically Slow Operator Dynamics in Constrained Many-Body Systems, Phys. Rev. Lett. **127**, 235301 (2021).
[56] T. Rakovszky, P. Sala, R. Verresen, M. Knap, and F. Pollmann, Statistical localization: From strong fragmentation to strong edge modes, Phys. Rev. B **101**, 125126 (2020).
[57] E. Guardado-Sanchez, A. Morningstar, B. M. Spar, P. T. Brown, D. A. Huse, and W. S. Bakr, Subdiffusion and Heat Transport in a Tilted Two-Dimensional Fermi-Hubbard System, Phys. Rev. X **10**, 011042 (2020).
[58] S. Pai, M. Pretko, and R. M. Nandkishore, Localization in Fractonic Random Circuits, Phys. Rev. X **9**, 021003 (2019).
[59] R. M. Nandkishore and M. Hermele, Fractons, Annu. Rev. Condens. Matter Phys. **10**, 295 (2019).
[60] M. Pretko, X. Chen, and Y. You, Fracton phases of matter, Int. J. Mod. Phys. A **35**, 2030003 (2020).
[61] M.-Y. Li and P. Ye, Fracton physics of spatially extended excitations. II. Polynomial ground state degeneracy of exactly solvable models, Phys. Rev. B **104**, 235127 (2021).
[62] C. Zhou, M.-Y. Li, Z. Yan, P. Ye, and Z. Y. Meng, Evolution of dynamical signature in the X-cube fracton topological order, arXiv:2203.13274.
[63] P. Sala, T. Rakovszky, R. Verresen, M. Knap, and F. Pollmann, Ergodicity Breaking Arising from Hilbert Space Fragmentation in Dipole-Conserving Hamiltonians, Phys. Rev. X **10**, 011047 (2020).
[64] V. Khemani, M. Hermele, and R. Nandkishore, Localization from Hilbert space shattering: From theory to physical realizations, Phys. Rev. B **101**, 174204 (2020).
[65] S. Moudgalya, A. Prem, R. Nandkishore, N. Regnault, and B. A. Bernevig, Thermalization and its absence within Krylov subspaces of a constrained Hamiltonian, in *Memorial Volume for Shoucheng Zhang*, edited by B. Lian, C. X. Liu, E. Demler, S. Kivelson, and X. Qi (World Scientific, Singapore, 2021), Chap. 7, pp. 147–209.
[66] Z.-C. Yang, F. Liu, A. V. Gorshkov, and T. Iadecola, Hilbert-Space Fragmentation from Strict Confinement, Phys. Rev. Lett. **124**, 207602 (2020).
[67] K. Lee, A. Pal, and H. J. Changlani, Frustration-induced emergent Hilbert space fragmentation, Phys. Rev. B **103**, 235133 (2021).
[68] S. Moudgalya and O. I. Motrunich, Hilbert Space Fragmentation and Commutant Algebras, Phys. Rev. X **12**, 011050 (2022).
[69] B. Mukherjee, D. Banerjee, K. Sengupta, and A. Sen, Minimal model for Hilbert space fragmentation with local constraints, Phys. Rev. B **104**, 155117 (2021).
[70] C. M. Langlett and S. Xu, Hilbert space fragmentation and exact scars of generalized Fredkin spin chains, Phys. Rev. B **103**, L220304 (2021).
[71] B. Pozsgay, T. Gombor, A. Hutsalyuk, Y. Jiang, L. Pristyák, and E. Vernier, Integrable spin chain with Hilbert space fragmentation and solvable real-time dynamics, Phys. Rev. E **104**, 044106 (2021).
[72] L. Herviou, J. H. Bardarson, and N. Regnault, Many-body localization in a fragmented Hilbert space, Phys. Rev. B **103**, 134207 (2021).
[73] A. Khudorozhkov, A. Tiwari, C. Chamon, and T. Neupert, Hilbert space fragmentation in a 2D quantum spin system with subsystem symmetries, arXiv:2107.09690.
[74] X. Feng and B. Skinner, Hilbert space fragmentation produces an effective attraction between fractons, Phys. Rev. Research **4**, 013053 (2022).
[75] W.-H. Li, X. Deng, and L. Santos, Hilbert Space Shattering and Disorder-Free Localization in Polar Lattice Gases, Phys. Rev. Lett. **127**, 260601 (2021).

[76] P. Patil and A. W. Sandvik, Hilbert space fragmentation and Ashkin-Teller criticality in fluctuation coupled Ising models, Phys. Rev. B **101**, 014453 (2020).
[77] J. M. Deutsch, Quantum statistical mechanics in a closed system, Phys. Rev. A **43**, 2046 (1991).
[78] M. Srednicki, Chaos and quantum thermalization, Phys. Rev. E **50**, 888 (1994).
[79] M. Rigol, V. Dunjko, and M. Olshanii, Thermalization and its mechanism for generic isolated quantum systems, Nature (London) **452**, 854 (2008).
[80] Z. Yan, Y. Wu, C. Liu, O. F. Syljuåsen, J. Lou, and Y. Chen, Sweeping cluster algorithm for quantum spin systems with strong geometric restrictions, Phys. Rev. B **99**, 165135 (2019).
[81] Z. Yan, Global scheme of sweeping cluster algorithm to sample among topological sectors, Phys. Rev. B **105**, 184432 (2022).
[82] See Supplemental Material at http://link.aps.org/supplemental/10.1103/PhysRevB.106.L041115 for a review of the height representation, examples of hQDM of various $m$ and interaction ranges, analytical tractable limits in the phase diagram, structure of Hilbert space, mapping between hQDM and spin models, single mode approximation within sweeping cluster QMC, and numerical data on correlation functions and structure factors.
[83] D. A. Huse, Z. Yan, Z. Y. Meng, and A. Chan (unpublished).
[84] Z. Yan, Z. Zhou, O. F. Syljuåsen, J. Zhang, T. Yuan, J. Lou, and Y. Chen, Widely existing mixed phase structure of the quantum dimer model on a square lattice, Phys. Rev. B **103**, 094421 (2021).
[85] The first-order phase transition is more easily understood using the exact mapping between the minimal-range hQDM and the two-dimensional XXZ model on the square lattice. In this XXZ model, this transition corresponds to the transition from Ising order $Jz > J_{xy}$ to the XY order $Jz < J_{xy}$, at the transition point $Jz = J_{xy}$ (corresponding to $V/t = -1$), the exact $O(3)$ symmetry of the model is recovered, and the ground state therein spontaneously breaks this symmetry and gives rise to a finite order parameter both in the Ising and the XY channels. The transition point is first order as both order parameters are finite. The situation is described in detail in Ref. [86].
[86] B. Zhao, P. Weinberg, and A. W. Sandvik, Symmetry-enhanced discontinuous phase transition in a two-dimensional quantum magnet, Nat. Phys. **15**, 678 (2019).
[87] G. Sun, N. Ma, B. Zhao, A. W. Sandvik, and Z. Y. Meng, Emergent O(4) symmetry at the phase transition from plaquette-singlet to antiferromagnetic order in quasi-two-dimensional quantum magnets, Chin. Phys. B **30**, 067505 (2021).
[88] O. F. Syljuåsen and A. W. Sandvik, Quantum Monte Carlo with directed loops, Phys. Rev. E **66**, 046701 (2002).
[89] O. F. Syljuåsen, Directed loop updates for quantum lattice models, Phys. Rev. E **67**, 046701 (2003).
[90] F. Alet, S. Wessel, and M. Troyer, Generalized directed loop method for quantum Monte Carlo simulations, Phys. Rev. E **71**, 036706 (2005).
[91] R. Moessner and K. S. Raman, Quantum dimer models, in *Introduction to Frustrated Magnetism* (Springer, Berlin, 2011), pp. 437–479.
[92] A. M. Läuchli, S. Capponi, and F. F. Assaad, Dynamical dimer correlations at bipartite and non-bipartite Rokhsar–Kivelson points, J. Stat. Mech.: Theory Exp. (2008) P01010.
[93] R. Moessner and S. L. Sondhi, Three-dimensional resonating-valence-bond liquids and their excitations, Phys. Rev. B **68**, 184512 (2003).
[94] Excitations in the XXZ KS can be seen as a Goldstone mode in the ferromagnetic spin-1/2 Heisenberg model, and the power $z = 2$ can be obtained via a simple spin-wave approximation.
[95] E. Ardonne, P. Fendley, and E. Fradkin, Topological order and conformal quantum critical points, Ann. Phys. **310**, 493 (2004).
[96] J. Haah, Local stabilizer codes in three dimensions without string logical operators, Phys. Rev. A **83**, 042330 (2011).
[97] S. Vijay, J. Haah, and L. Fu, A new kind of topological quantum order: A dimensional hierarchy of quasiparticles built from stationary excitations, Phys. Rev. B **92**, 235136 (2015).
[98] S. Vijay, J. Haah, and L. Fu, Fracton topological order, generalized lattice gauge theory, and duality, Phys. Rev. B **94**, 235157 (2016).
[99] C. Chamon, Quantum Glassiness in Strongly Correlated Clean Systems: An Example of Topological Overprotection, Phys. Rev. Lett. **94**, 040402 (2005).
[100] M. Pretko, Generalized electromagnetism of subdimensional particles: A spin liquid story, Phys. Rev. B **96**, 035119 (2017).
[101] M. Pretko, Subdimensional particle structure of higher rank $u(1)$ spin liquids, Phys. Rev. B **95**, 115139 (2017).
[102] J. Feldmeier, F. Pollmann, and M. Knap, Emergent fracton dynamics in a nonplanar dimer model, Phys. Rev. B **103**, 094303 (2021).
[103] Y. You and R. Moessner, Fractonic plaquette-dimer liquid beyond renormalization, arXiv:2106.07664.
[104] https://www.paratera.com/.